Breakdown of two-phase random resistor networks

P. M. Duxbury

Department of Physics and Astronomy and Center for Fundamental Materials Research, Michigan State University,
East Lansing, Michigan 48824-1116

P. D. Beale

Department of Physics, University of Colorado, Boulder Colorado 80309

C. Moukarzel

Höchstleistungsrechenzentrum, Forschungszentrum, D-52425 Jülich, Germany

(Received 12 August 1994)

We describe the failure of two-component square- and cubic-lattice random resistor networks. The model behavior is dependent on the ratio of the conductances of the two components g, the ratio of the (brittle) failure thresholds of the two components i, the volume fraction p, and the sample size L. For much of the parameter space, the average strength of the networks shows a rather weak size effect, and a scaling argument suggests that this size effect is logarithmic. As usual, near the percolation points, there can be algebraic scaling provided i and g are very large or small. Near the limits $p = 0$ and $p = 1$, there is a logarithmic ("dilute-limit") singularity in average strength. The ability to absorb damage is very strongly dependent on the model parameters. When one phase is more conducting and weaker than the other, and the strong phase is connected, the damage is usually extensive. Basically most of the weak bonds fail prior to the failure of the whole network. In the other regions of parameter space, damage is not extensive, but it does sometimes scale in a nontrivial way with the sample size.

I. INTRODUCTION

Almost all materials are disordered, either due to randomly occurring point defects, dislocations, and grain boundaries, and/or due to a mixture of phases in their microstructure. To understand the properties of materials, it is essential to understand the effect of various impurities and microstructures on material response. Although elasticity, electrical conductivity, and many transport properties are dependent on the defects in the material, they are not usually as sensitive to defects as are instabilities such as dielectric failure, electrical failure, yield, and fracture. There is thus a broad classification of material properties into those that are "structure insensitive" and those that are "structure sensitive."

The distinction between structure-sensitive properties and structure-insensitive properties is clearly illustrated in network models for the transport and/or elastic properties and breakdown of randomly diluted brittle materials.[1] There it is known that structure-insensitive properties such as the elastic moduli,[2] conductivity,[3] and capacitance[4] can be treated perturbatively in the weak-disorder limit and exhibit scaling behavior near the percolation point. In contrast, structure-sensitive properties, such as fracture stress,[2] critical current,[3,5,6] and dielectric breakdown field,[4,7] can *not* be treated perturbatively in the weak-disorder limit as they exhibit a logarithmic singularity there. Indeed the distinction between structure-sensitive (or extreme) properties and structure-insensitive (or low-moment) properties has been linked to the way in which stress or electric field is carried in a disordered microstructure.[1] It is possible to calculate explicitly (numerically) the probability distribution of having a specified local load (either stress or electric field) in a bond of the network, and it has been shown that the elastic moduli, conductivity, and capacitance are related to the second moment of this distribution,[1] while brittle failure properties (fracture stress, critical current, dielectric breakdown field) are often related to the very high moments of this distribution.[1] Note that there are some failure problems, such as tensile failure of some ceramic-ceramic composites[8] and the critical current of strong-pinning superconductors,[9] where "mean-field theories" seem to work and hence which are structure insensitive.

Naturally, there has been far more progress in the development of methods to estimate the effective transport and elastic moduli and other low-moment properties than there has in estimating the average or effective breakdown properties. Nevertheless, there has been a great deal of work on breakdown properties due to their immense technological importance. More recently, there has been a burst of activity in this area, with modern ideas and methods such as fractals, the analysis of instabilities, scaling concepts, and large-scale numerical simulations (both statistical and electronic structure calculations) focused on this problem.[10,11] As always, it is important to develop a set of simple models which can be analyzed in detail and in which the basic concepts can be well illustrated. In the study of the effective transport[12,13] and elastic properties,[12,14] systems with a two-phase composite microstructure have played that role. In breakdown problems, many of the important scaling properties are captured in simple "quasi-one-dimensional" models.[15,16] However, there are important

effects due to the nontrivial way in which stress (or electric field) is distributed in higher dimensions and due to the constrained crack path imposed by one-dimensional models.

In this paper we report on a systematic study of the failure of two- and three-dimensional electrical networks consisting of two types of bonds, i.e., a random two-phase composite. There are several motivations for this study. First, we wish to illustrate the difference between low-moment and extreme-moment properties of random composites and to point to the difficulties in developing bounds and analytic estimates for the average strength. Secondly, we wish to compare the behavior of two- and three-dimensional models with similar microstructures to test the effect of dimensionality on failure behavior. And, thirdly, we want to determine the microstructures which optimize strength and damage tolerance. By using the analogies stress→current and strain→voltage, the results found here can also be used to develop understanding of the mechanical response of random structural composites. One must, of course, keep in mind the absence of shear in these simple models of mechanical response, but in many ways these electrical models are more sophisticated than the quasi-one-dimensional models often used in the analysis of the mechanical response of composites.

The paper is organized as follows. In the next section we introduce the model and some simple reduced variables used to describe its properties. In this section we also discuss the numerical method we used, some methods of averaging the current-voltage relationships and their pitfalls, and some useful measures of breakdown that can be extracted from the current-voltage relationships. In Sec. III, we present results of simulations of two- and three-dimensional networks. In this section we also describe analytic arguments that help qualitatively and semiquantitatively explain some of the numerical data. There are two appendixes which contain much of the detailed analytic analysis. In Sec. IV, we summarize the main results of the paper, and respond to the detailed motivations outlined in the previous paragraph. One aspect of the three-dimensional model is presented in a separate paper.[17] In Ref. 17, we compare the properties of a particulate composite (i.e., in a regime where only one phase in a cubic lattice is connected) with the behavior of an interpenetrating-phase composite (i.e., in a regime where both phases are percolating). In Ref. 17 we also discussed in detail the numerical procedure and averaging procedures we use here, so some parts of Sec. II of this paper are brief.

II. THE MODEL, FAILURE ALGORITHMS, AND AVERAGING PROCEDURES

The model

We consider square and cubic lattices, whose bonds are randomly chosen to be one of two types of brittle fuses. Initially, each bond has a conductance and a threshold current beyond which it fails irreversibly and carries no current. Before failure begins, a fraction p of the bonds (which we always refer to as *matrix* bonds) has conductance g_0 and a current threshold i_0, while the other $(1-p)$ of the bonds *(inclusion* bonds or simply inclusions) have conductance g_1 and threshold i_1. The linearity of the problem implies that the failure behavior of any such random mixture of bonds is equivalent, up to a rescaling of currents and voltages, to a system where matrix bonds have conductance and threshold unity, and inclusion bonds have conductance $g=g_1/g_0$ and threshold $i=i_1/i_0$. The model also transforms into itself if matrix and inclusion bonds are interchanged and suitably rescaled. That is, the model maps into itself if

$$p \rightarrow 1-p, \quad i \rightarrow 1/i, \quad \text{and } g \rightarrow 1/g . \tag{1}$$

Note that for a given random configuration this transformation leads to a *different random configuration* with nominally the same values of p, g, and i. The transformation thus gives a statistically equivalent system, but not one that is equivalent for each member of an ensemble. For two key quantities that we consider, I_b (the average of the peak current in the current-voltage curves) and the damage n_b (the average number of bonds broken before the peak of the current-voltage curves), the transformation (1) leads to the transformed quantities I_b' and n_b' by

$$I_b' = \frac{I_b}{i} \quad \text{and } n_b' = n_b . \tag{2}$$

For the square lattice the percolation threshold is 0.5 for all lattice sizes. On the cubic lattice[18] for $p < 0.2488$, the inclusion phase is connected across the sample, but the matrix phase is not, for $0.2488 < p < 0.7512$ both the inclusion and matrix phases are macroscopically connected and percolate across the system (the interpenetrating-phase regime), and for $p > 0.7512$ only the matrix phase is connected and the inclusions form isolated clusters in the connected background matrix.

Failure algorithms and averaging procedures

A "quasistatic" breaking process can be numerically simulated by means of the "hottest-bond (HB) algorithm,"[19] which consists of removing at each time step the most loaded bond from the system, and recalculating the whole distribution of currents after each bond removal. Physically, this corresponds to very slow nucleation of cracks and other defects, and is appropriate when the failure process is quasistatic so that the dynamics of load redistribution after local failure is not important (At the opposite extreme is fast fracture or impact, where the dynamics is of paramount importance, and methods such as molecular dynamics are more appropriate.) The load of a bond is defined as the quotient between the current which flows through it and its failure threshold.

The hottest-bond algorithm is computationally slow, as the whole current distribution has to be recalculated after each bond removal. This imposes a severe limitation on the sizes one is able to simulate with this algorithm, so to analyze bigger systems, we developed an alternative method, which we call the multiple-hottest-bond (MHB) algorithm and which is defined as follows. The voltage is fixed to a given value and *all bonds which surpass their*

critical current are removed. The currents are then recalculated and eventually more bonds are removed at the same voltage. This is repeated until no more bonds are broken at this voltage. At this point the voltage is increased in small steps and the whole procedure repeated until the sample is broken apart. The advantage of this algorithm is that many bonds can be removed each time the equations are solved, diminishing the computational load needed to break the sample. On the other hand, if the voltage steps are small we have found that, in the regime prior to the peak of the *I-V* curve, the current-voltage characteristics found with this method are very close to those found using the hottest-bond algorithm. We also checked that the damage prior to peak and the value of the failure current and voltage were accurate to better than 5%.

The current distribution is calculated iteratively by means of the conjugate gradient (CG) method,[15] and we found that the error criterion

$$\Delta = \frac{\sum_{ij}[f_{ij}(t) - f_{ij}(t-10)]^2}{\sum_{ij}f_{ij}^2(t)} \tag{3}$$

provides an excellent measure of convergence. Here $f_{ij} = i_{ij}/I_{ij}$, is the current flowing through a bond and I_{ij} is its failure threshold. Sufficient accuracy is achieved with the condition $\epsilon > \Delta$, with ϵ typically 10^{-4} (for a more detailed discussion, see Ref. 17).

There are a variety of averaging procedures that can be applied to an ensemble of current-voltage relationships such as that shown in Fig. 1. However, we have found that *averaging the current-voltage curves can lead to misleading results* concerning the shape of the typical current-voltage characteristics, and in particular the values of I_b found from such averaged curves are *consistently and sometimes much lower* than the typical values found in each member of the ensemble (for a detailed discussion, see Ref. 17). We thus present current-voltage curves for single configurations, and the averages are done after extracting an interesting quant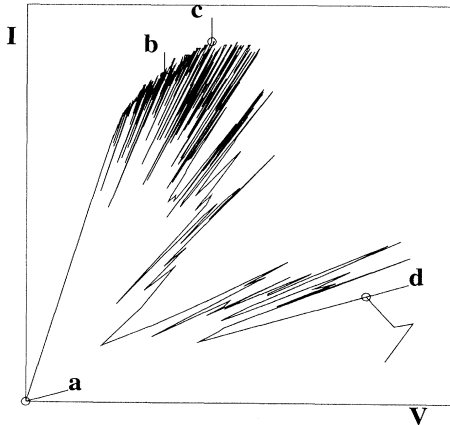ity from each member of the ensemble. Surprisingly, there appears to be no need to average the current-voltage relationships anyway, as members of the ensemble have current-voltage curves which are similar to each other, as will be seen below.

Important measures of strength, damage, and toughness

In studying failure evolution, it is possible to study the geometry of crack evolution and the geometry of the final damage path, and/or the current-voltage curve and quantities derived from it. The final crack path and the post-peak behavior of the current-voltage curve are very sensitive to the failure algorithm used. In this regime, different crack evolution algorithms and loading conditions lead to very different failure paths. This "unstable regime" has been the focus of much recent interest but is not the focus of study here.[20] In contrast, the prepeak behavior is more stable, and is less sensitive to the chosen algorithm and loading conditions. This is the regime of major interest here. This is also the regime of technological importance.

A typical current-voltage relationship is presented in Fig. 1. The damage states at points $a-d$ of Fig. 1 are presented in Figs. 2. It is seen from Figs. 2(a)–2(c) that damage is random early in the failure process, and even at point c, at which the breakdown instability occurs, the damage is quite random. It is only after the peak of the I-V curve that the damage becomes localized [see Fig. 2(d)]. From curves such as Fig. 1, it is possible to define a variety of interesting physical quantities. The initial linear slope gives the effective conductance of the composite $g_{\rm eff}$. There are also the number of inclusion bonds that have failed at peak (the inclusion damage $n_{\rm inc}$), and the number of matrix bonds that have failed at peak (the matrix damage $n_{\rm mat}$). The sum of these two is the total damage n_b. Since the power required to break the two components of the composites can be very different it makes sense to define a "weighted damage,"

$$n_w = \frac{n_{\rm inc}v_{\rm inc}^2 g_{\rm inc} + n_{\rm mat}v_{\rm mat}^2 g_{\rm mat}}{v_{\rm inc}^2 g_{\rm inc} + v_{\rm mat}^2 g_{\rm mat}}$$

$$= \frac{n_{\rm inc}i^2/g + n_{\rm mat}}{i^2/g + 1}. \tag{4}$$

Here, $v_{\rm inc}$ is the breakdown voltage in an inclusion bond and $v_{\rm mat}$ is the breakdown voltage of a matrix bond. The damage itself has the disadvantage that it just counts the number of broken bonds, regardless of whether it was easy or hard to break them. The weighted damage corrects this by weighting each failed bond with the power required to break it. Also, the normalization in the definition of the weighted damage (4) ensures that n_w is symmetric under the transformation (1). We thus prefer the weighted damage as a good *scalar* measure of the ability of the lattice to absorb damage. The strength of the composite is characterized by the current at peak (point c of Fig. 1), I_b. In this paper we shall concentrate on the quantities $g_{\rm eff}$, I_b, and n_w. One additional current scale that is important in the analysis is the applied current I_i at which the *first* bond in the composite fails.
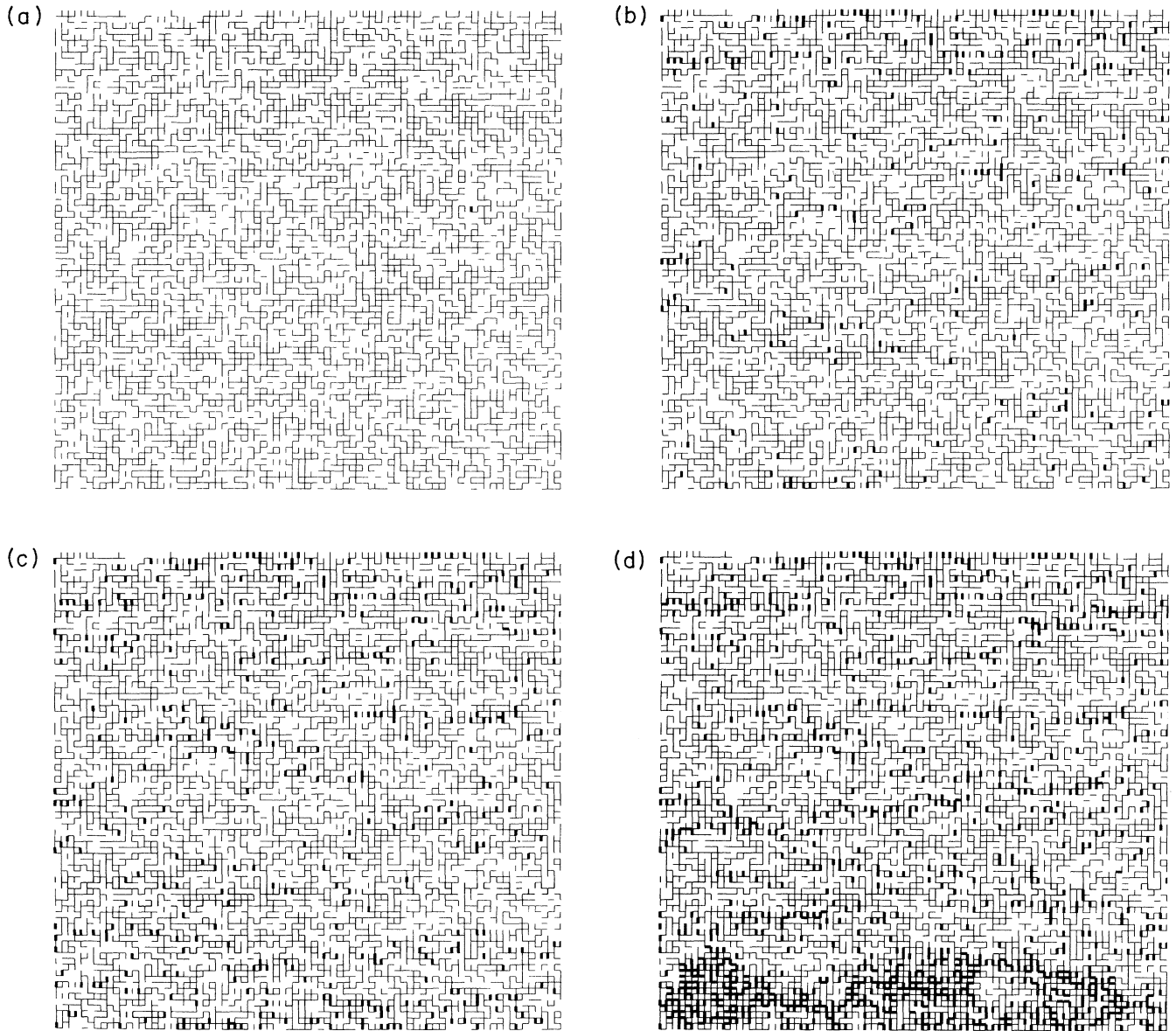
FIG. 1. A typical *I-V* curve for an 80×80 square lattice with $p = 0.50$, $g = 8$, and $i = \frac{1}{4}$.

FIG. 2. The damage at points (a) a, (b) b, (c) c, and (d) d of Fig. 1. It is seen from these figures that the damage is quite random up to the instability point c. Dotted lines are inclusions, full lines are matrix, and thick lines are broken bonds.

Note that the current and voltages we use are normalized by the cross-sectional area (in the case of currents) and the length (in the case of voltage) so in the continuum limit they correspond to the current density and the electric field, respectively.

III. RESULTS

The typical I-V relationships of two-dimensional (2D) systems are presented in Fig. 3 for a range of values of g and i. In Fig. 3(a), we give data at $p = 0.75$, while in Fig. 3(b) we give data at $p = 0.50$. It is seen that, in Fig. 3(a), there is little damage prior to the peak of the I-V curve

for small g and large i, while for large g and small i there is considerable damage. In contrast, at $p = 0.5$ there is damage prior to peak whenever g/i is considerably different than unity. Figure 3(b) must have approximate symmetry under Eq. (1). This symmetry is seen more clearly in averaged quantities, such as the average weighted damage present in the contour plots of Figs. 4 and 5. In all cases, the primary source of damage is the failure of the weak phase of the composite. Damage is maximal when the strong phase is connected and the weak phase is highly conducting, as then current is channeled into the weak phase and damage is enhanced. As shown in Fig. 6, damage is extensive in the weak-phase
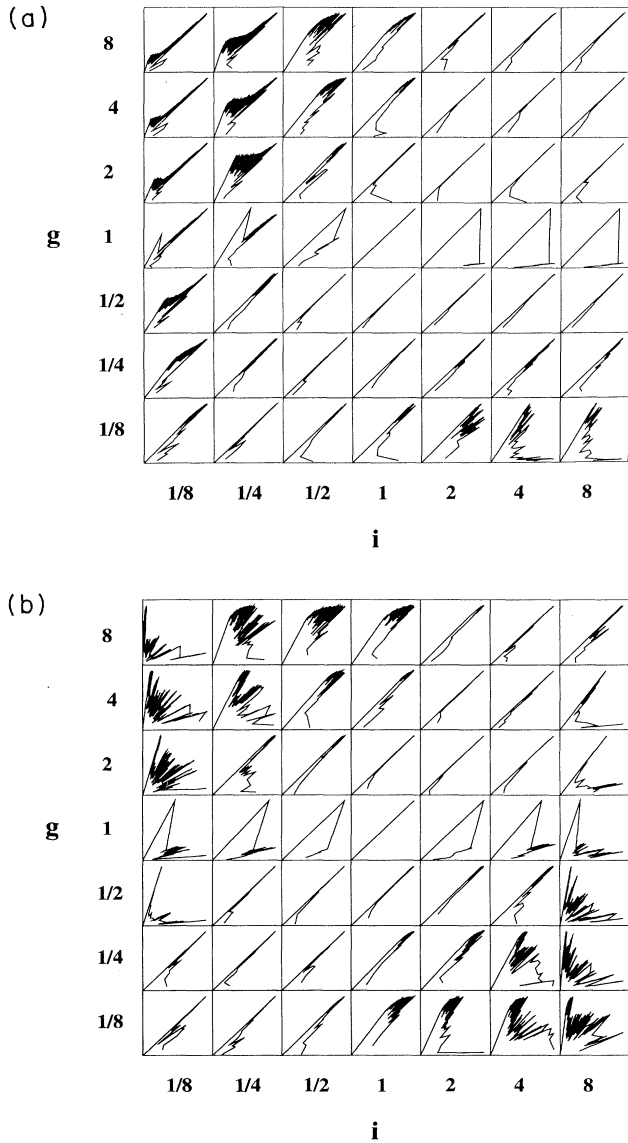
(a)

(a)

(b)

(b)

FIG. 3. The typical I-V curves for one sample of $L = 100$ square lattices for a range of values of g and i for (a) $p = 0.75$ and (b) $p = 0.50$. The scales are not the same for each curve.

FIG. 4. Weighted damage (n_w) maps (see text) for $L = 100$ square lattices at (a) $p = 0.75$ and (b) $p = 0.50$. The averages are over 10 configurations. The white level corresponds to $n_w < 8.3$ (a), and 4.5 (b), while the darkest level corresponds to $n_w > 91.2$ (a) and 49.5 (b), and the gray scale is linear.

damage regions of Fig. 4. In 2D, the amount of damage in the weak phase is much smaller at p_c than for $p = 0.75$ (see Fig. 4), and in 3D, the most damage occurs in the center of the interpenetrating phase regime $p = 0.5$ (see Fig. 5). The damage n_b shows similar behavior in the regime considered in the plots of Figs. 4 and 5, but shows a different behavior when i^2/g is very small, as there the weighted damage in the inclusion phase is much smaller than the damage n_b.

There is a matrix damage mechanism which produces some stable matrix damage when g is large, i is large, and the strong phase is *disconnected* [i.e., in the upper right corners of Figs. 4(a) and 5(a)]. This damage mechanism is due to the fact that a highly conducting strong inclusion induces failure at its ends, but the failed region at
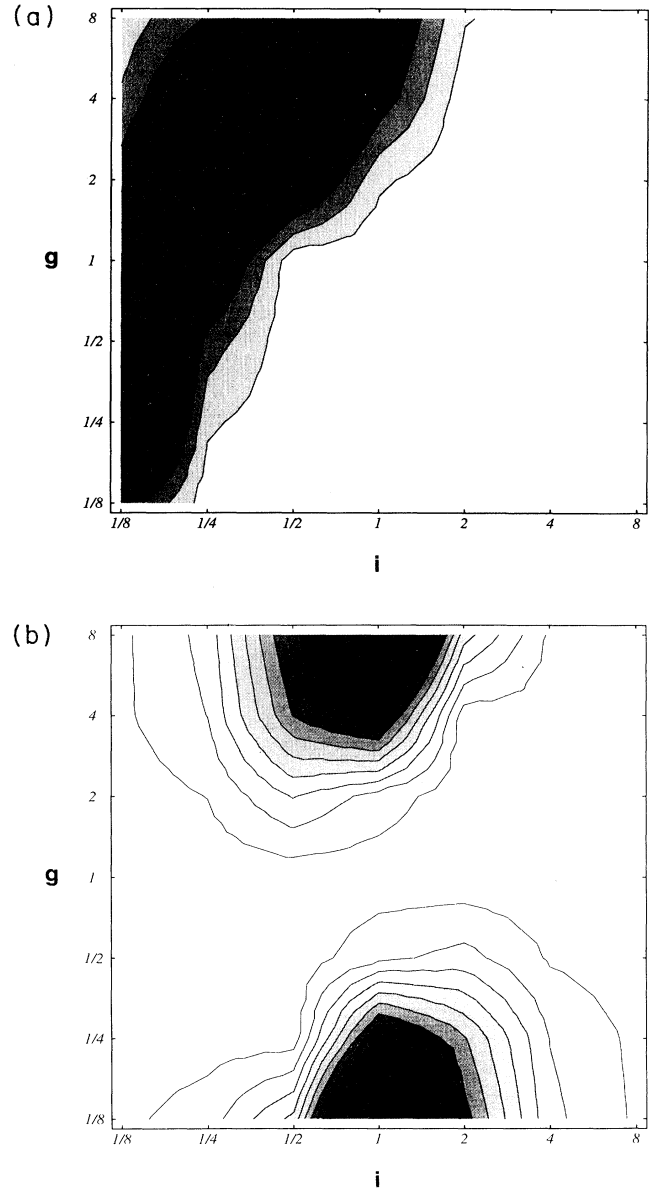
the end of the inclusion shields the inclusion tip. A crack initiated from a "needle tip" must propagate transverse to the region of high initial current concentrations. This geometric constraint leads to some stable localized damage near needle tips for g, i, and p large. A scaling analysis (see Appendix B) suggests that in this regime the matrix damage scales as

$$n_b \sim n_w \sim L^x \quad \text{with} \quad x = d[1 - (I_i/I_b)^{2/\nu}] \, , \qquad (5)$$

where for a single needle I_i is the applied current scale at which the region near the needle tip fails, while I_b is the
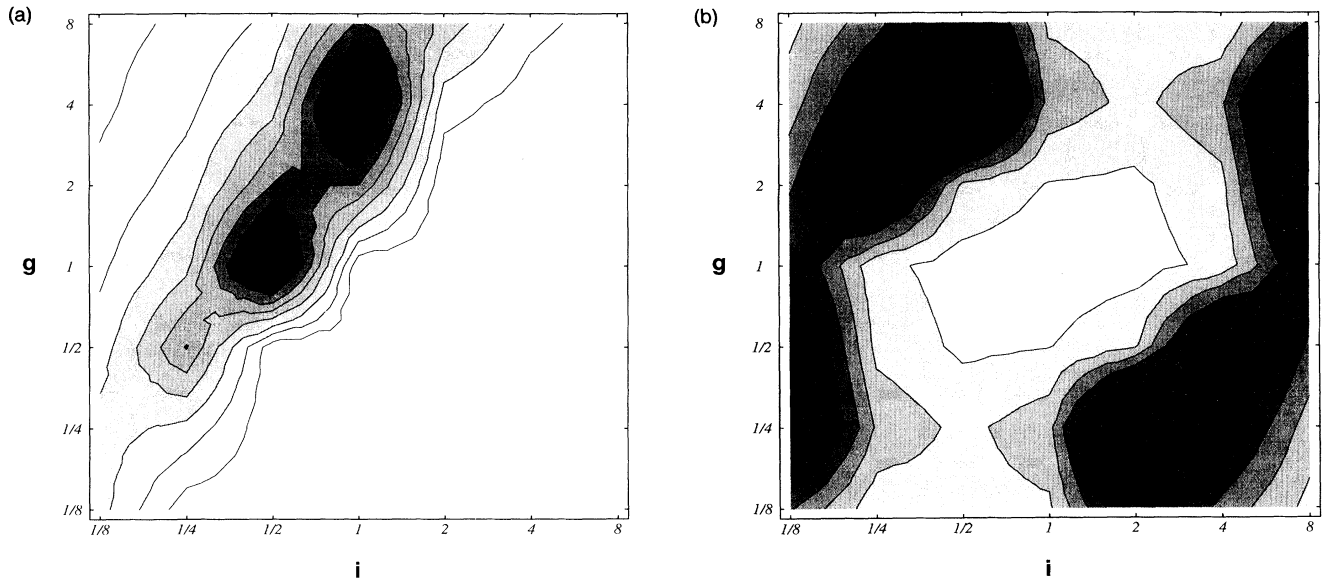
FIG. 5. Weighted damage (n_w) maps (see text) for cubic lattices at (a) $p=0.85$ ($L=15,20$ configurations) and, (b) $p=0.50$ ($L=20,10$ configurations). The white level corresponds to $n_w < 9.17$ (a) and 20.5 (b), while the darkest level corresponds to $n_w > 100.8$ (a) and 225.5 (b), and the gray scale is linear.
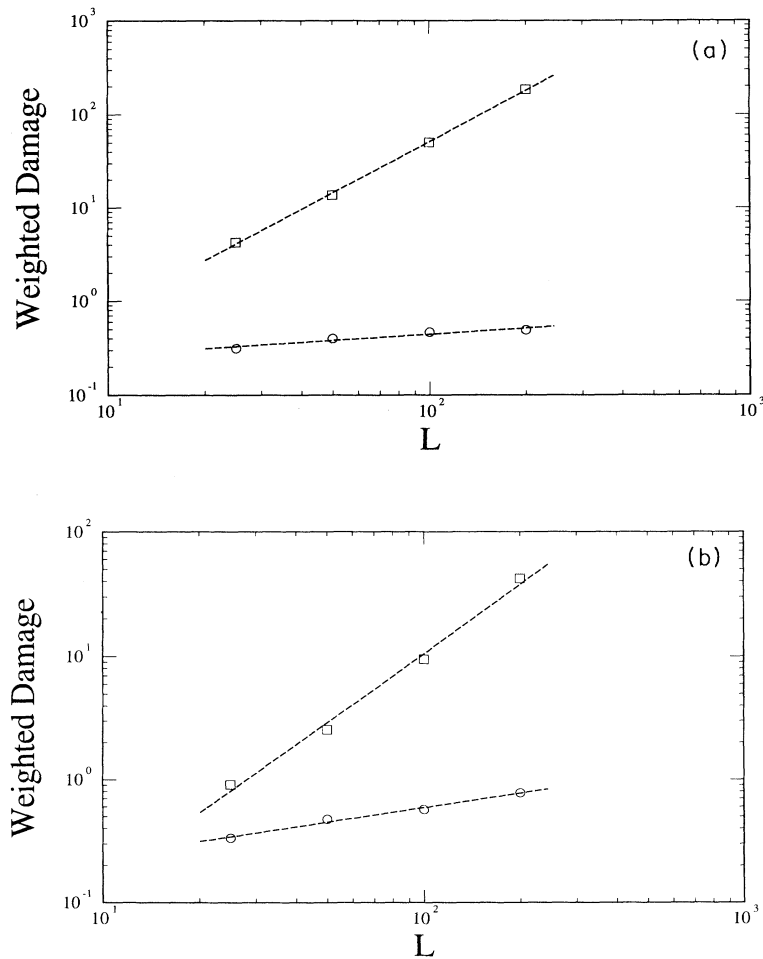

FIG. 6. The finite-size scaling behavior of the weighed damage n_w at (a) $p=0.75$ (the square symbols have exponent close to 2) and (b) $p=0.50$ (the open circles give exponent less than 1). In both cases the squares are for $g=4, i=\frac{1}{4}$, while the circles are for $g=4.0, i=4.0$.
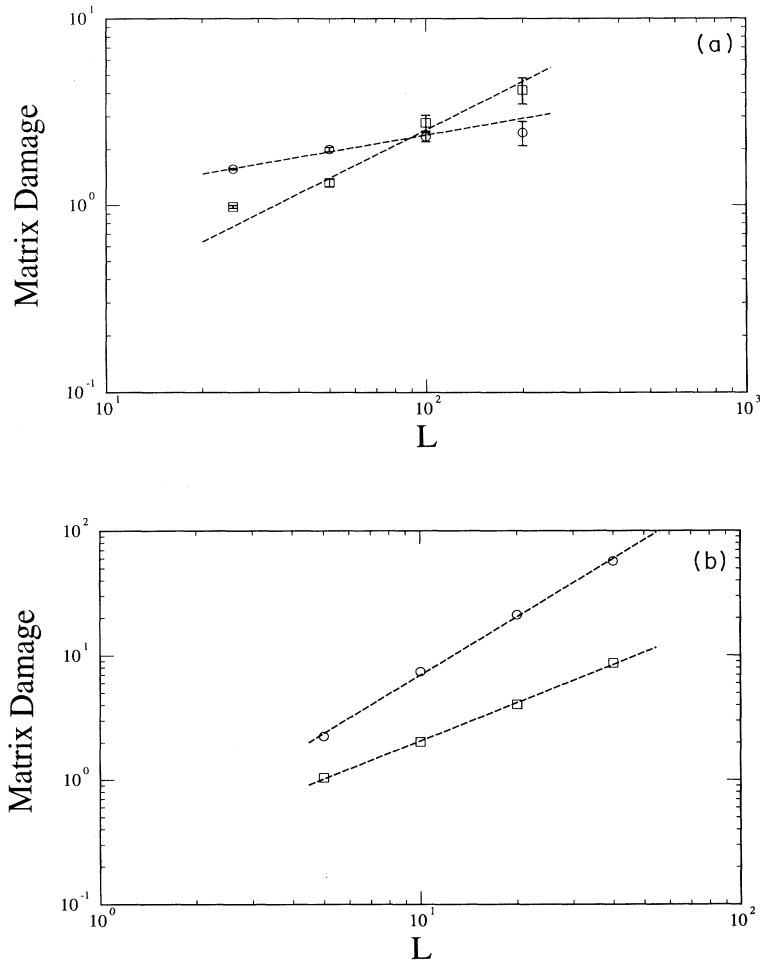
FIG. 7. Finite-size scaling behavior of the matrix damage at (a) $p=0.75$ for square lattices and (b) at $p=0.85$ for cubic lattices. In both cases the squares are for $g=4, i=\frac{1}{4}$, while the circles are for $g=4.0, i=4.0$, Both of the exponents in (a) are less than 1, while the circles and squares in (b) give exponents 1.55 ± 0.1 and 1.0 ± 0.1, respectively.

applied current scale at which the transverse crack propagates. The scaling analysis of Appendix B shows how these quantities are defined in the random network case. Numerical results for the matrix damage at $p=0.75$ in 2D and for matrix damage at $p=0.85$ in 3D are presented in Fig. 7, where it is seen that a nontrivial exponent exists in the 3D case, while in 2D this "tip-sealing" mechanism is less effective. This is reasonable, as stress concentration effects are less severe in 3D than in 2D. The damage due to this mechanism is quite random, and the damage estimate in Eq. (5) does not include the bonds broken after the peak of the I-V curve.

It has been shown that, in many models of disordered systems, there is a logarithmic size effect in the average strength[5,16,21] (I_b in this model). We thus tested the scaling behavior of the critical current in this model, and the results are presented in Fig. 8 for the 2D case. In all cases in this figure, an algebraic fit to the data gives an exponent less than 0.15, while a logarithmic fit gives an exponent of order 0.5 ± 0.5. In all cases the size effect is very weak, and it is not possible to distinguish reliably between an algebraic law and a logarithmic one. In fact, one might claim that there is no size effect in these models as the two components have finite strength. If the

conductances are all the same there is certainly no size effect. However, when the moduli are different, there are defect clusters which produce current enhancements which grow algebraically with the cluster size (in the limit of one phase being a void, for example, cracklike defects give the exponent $\frac{1}{2}$). For general g, a funnel defect was shown to have this property,[22] and it is straightforward to show (see Appendix A) that wedge defects do too. Failure at the tip of a wedge defect leads to unstable crack growth, and so it plays the same role a crack does in the void limit. A simple scaling argument (see Appendix A) then shows that in the regime where the defect clusters are isolated, one expects a very weak logarithmic size effect,

$$I_b \sim \frac{I_0}{1+k(\ln L)^{\nu/2}}, \tag{6}$$

where $0<\nu/2<1$, and in fact $\nu/2$ is usually expected to be less than 0.5 (see below). The argument leading to Eq. (6) is a simple extension of the argument of Duxbury, Leath, and Beale [5] for the case of weakly diluted lattices. This argument identifies defects which are likely to be typical of those inducing failure in random networks.
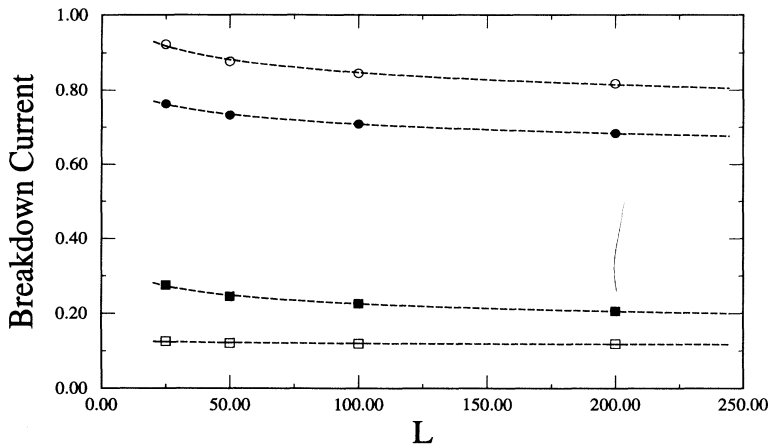
FIG. 8. Finite-size scaling behavior of the average breakdown current for square lattices at $p=0.75$ (solid symbols) and $p=0.50$ (open symbols). Squares are for $g=4, i=\frac{1}{4}$, while circles are for $g=4.0, i=4.0$. For $L=25,50,100,200$, the averages are over $2500,500,100,20$ configurations, respectively.

In the random networks considered here, wedges and funnels lead to strong local current concentrations, and so analysis of these defects leads to an estimate of the applied current at which failure occurs. Using a wedge as the failure-inducing defect (see Appendix A) leads to (in 2D)

$$v_w = 1 - \frac{2}{\pi}\cos^{-1}\left[\frac{1-g}{2+2g}\right] \quad \text{for } g < 1 , \tag{7}$$

while an analysis based on a funnel defect predicts (see Appendix A)

$$v_f = 1 - \frac{4}{\pi}\tan^{-1}(g^{1/2}) \quad \text{for } g < 1 . \tag{8}$$

Since the maximum value of v is 1, the scaling exponent implied by funnels and wedges is less than $\frac{1}{2}$. This is in contrast to the void limit where cracks are the most important defects, and the scaling exponent may be 1. Numerical work supports these exponents,[23] but also shows that there are strong size effects, so that for most of the same sizes considered the observed value can be somewhat higher than predicted by Eqs. (7) and (8). In three dimensions, solids of revolution formed from funnels and wedges lead to strong current concentrations; however, since the volume of these defects scales as the linear size cubed, l^3, the asymptotic scaling exponent in the size effect, $v/3 < \frac{1}{3}$. Nevertheless, the important prediction is that a weak logarithmic size effect persists in particulate composites for most values of g and i. Surprisingly, in the interpenetrating-phase regime and at p_c, the size effect is also very weak, at least for g and i not too large. However, in the void case ($i^2/g \rightarrow 0$), $I_b \sim 1/L^{d-1}$ at p_c, so there is a strong size effect in that limit (for example, we have checked that for square lattices at p_c, with $g=100$, and $i=0.01$, $I_b \sim 1/L$).

The dependence of the breakdown current, conductance, and damage on volume fraction p is presented in Figs. 9–12. In Figs. 9, we compare the behavior of 2D and 3D systems for intermediate values of g and i. There it is seen that there is a pronounced drop in strength for p near 0 and for p near 1, with this feature being more pro-

nounced in 2D than in 3D. This "dilute-limit singularity" has been studied extensively before in fracture,[2] dielectric breakdown,[4] as well as for fuse networks,[5] and is predicted by the simple scaling Eq. (A9) of Appendix A [$a \ln(1-p)$ behavior on approach to $p=1$]. In Figs. 9, there is always an intermediate value of p at which I_b is a minimum. Note that this minimum does not occur at 0, 1, or p_c. This minimum is especially pronounced in 3D [see Fig. 9(b)]. The absence of a strong size effect at p_c is also evident in Figs. 9, where it is seen that for all values of p the size effect is quite weak. The dependence of I_b on p naturally becomes much stronger when g and i are large as seen in Figs. 10. Then, there are quite strong features near the percolation point, at which the "strong" phase first connects. After correcting for the different percolation thresholds in 2D and 3D, the behavior of Figs. 10(a) and 10(b) is quite similar. The strong size effect near p_c is also evident. When g and i are large, the dilute-limit singularity is still present, but is obscured by the strong dependence on p near p_c. There is again a value of $p \neq p_c$ at which the strength is a minimum. For comparison, the effective conductance g_{init} as a function of p is presented in Fig. 11. There is a linear behavior near $p=0$, and a monotonic decrease in the effective conductance in interpolating between $p=0$ and $p=1$.

The weighted damage as a function of p is presented in Figs. 12. It is seen from these figures that there is no strong feature near the percolation point, in either 2D [Fig. 12(a)] or 3D [Fig. 12(b)]. Instead, there is often a maximum in the damage at some intermediate value of p. Most damage occurs when one phase is weak and highly conducting compared to the other, i.e., in cases where $g=4$, $i=\frac{1}{4}$, and $p>\frac{1}{2}$, or $g=\frac{1}{4}$, $i=4$, and $p<\frac{1}{2}$. It is also seen [see Fig. 12(b)] that in regions where the damage is large there is a strong size effect in the damage, and Figs. 6 showed in these regions the damage is usually extensive. If i^2/g is very small, the damage remains extensive, but the weighted damage is smaller. This is because the bonds that are failing are very weak. The maximum weighted damage thus occurs at intermediate values of g and i as seen in the damage maps of Figs. 4 and 5.
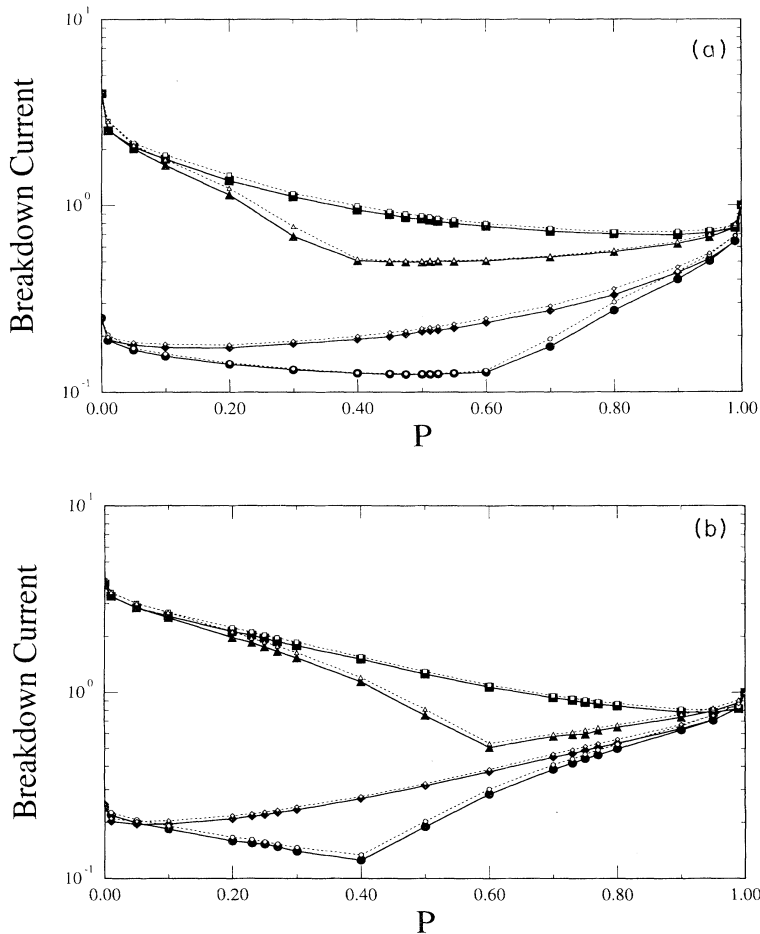
FIG. 9. The average breakdown current of (a) square and (b) cubic lattices, as a function of the concentration p of the matrix phase. Squares indicate $g=4, i=4$, triangles are for $g=1/4, i=4$, diamonds are for $g=\frac{1}{4}, i=\frac{1}{4}$, and circles are for $g=4, i=\frac{1}{4}$. In (a), the open symbols are for $L=50$ (50 configurations), while the solid symbols are for $L=100$ (20 configurations). In (b), the open symbols are for $L=10$ (50 configurations), while the solid symbols are for $L=20$ (20 configurations).

IV. SUMMARY AND DISCUSSION

We have presented a comprehensive study of the failure of two- and three-dimensional two-phase random electrical networks. Some of the key trends observed are the following.

(1) The damage is quite random up to the instability point (see Fig. 2).

(2) For most values of p there is an intermediate value of g and i at which the damage tolerance is optimal (see Figs. 4 and 5). In these regimes, the damage is extensive (see Figs. 6).

(3) For most values of p, g, and i, the size effect in the average strength is very weak (Fig. 8), and a scaling argument suggests that in the "particulate" regimes the size effect is asymptotically of the form $1/(\ln L)^{\beta}$, with the exponent β often less than $\frac{1}{2}$. Near the percolation points, and only for extreme values of g and i, the size effect is of order $1/L$.

(4) There is always a pronounced reduction in strength for p close to 0 and 1 (see Figs. 9 and 10). A scaling argument suggests that this dilute-limit singularity is logarithmic [see Eq. (16)].

(5) In contrast to the average conductance (see Fig. 11), the average strength (see Figs. 9 and 10) does not

behave monotonically as a function of p. Even when the inclusions that are added are stronger than the matrix, quite a high volume fraction of inclusions must be added before the composite strength exceeds the strength of the matrix.

(6) The strength of composites is higher if $g \sim i$ (see Fig. 9), while the damage is enhanced when g is quite different than i (see Figs. 4 and 5). As is often the case, optimal strength and optimal damage tolerance do not occur for the same microstructure.

Although we have learned a great deal about these composites from the scaling analysis and simulations described here, a simple theory for the dependence of strength on p for general p, g, i, and L is lacking (e.g., Figs. 9 and 10). Due to the importance of funnels and other stress-concentrating defects, it is unlikely that a simple quasi-one-dimensional "chain-of-bundles" model can capture the essence of this model. Certainly the simplest rule-of-mixtures prediction $[I_b = pI_0 + (1-p)I_1]$ is grossly inadequate, and it is a challenge to include the dilute-limit singularity and the size effect in a comprehensive theory. In fact, in the infinite-lattice limit the strength is zero everywhere except in the homogeneous limits, so the analysis must always include a size-effect factor. This is in contrast to bounds on low-moment properties such as conductance and strength,[24] which are
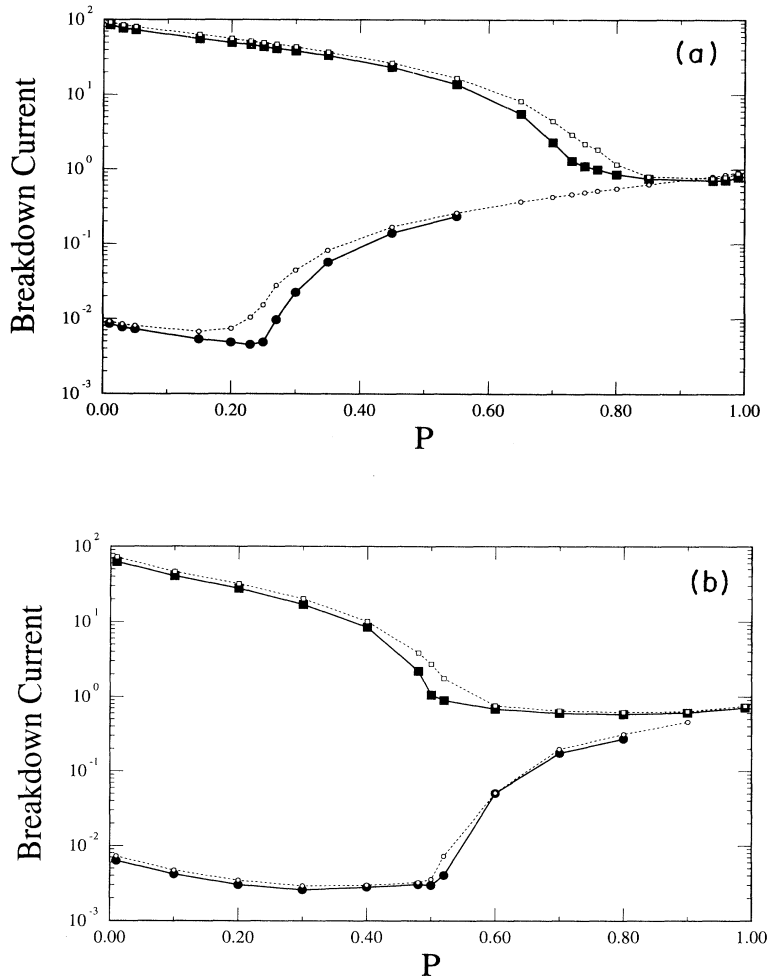
FIG. 10. The average breakdown current of (a) square and (b) cubic lattices, as a function of the concentration p of the matrix phase. Squares indicate $g=100, i=100$ and circles are for $g=100, i=\frac{1}{100}$. In (a), the open symbols are for $L=50$ (50 configurations), while the solid symbols are for $L=10$ (20 configurations). In (b), the open symbols are for $L=10$ (50 configurations), while the solid symbols are for $L=20$ (20 configurations).

now sophisticated and accurate, but are simpler in the sense they are size independent and do not have to contend with the dilute-limit singularity.

The qualitative ideas concerning the composite behavior are quite similar in 2D and in 3D. The weaker current concentration effects in 3D are reflected in a weaker dilute-limit singularity, and the fact that the tip-sealing matrix damage mechanism is stronger in 3D than in 2D. In 3D, damage is often a maximum in the interpenetrating-phase regime in which both of the phases percolate [see Fig. 12(b)]. This phase does not exist in 2D, and there the maximum damage occurs at intermediate values of p.

Finally, in most materials, there are several other important factors affecting composite behavior. Certainly the interface between matrix and inclusion is another im-
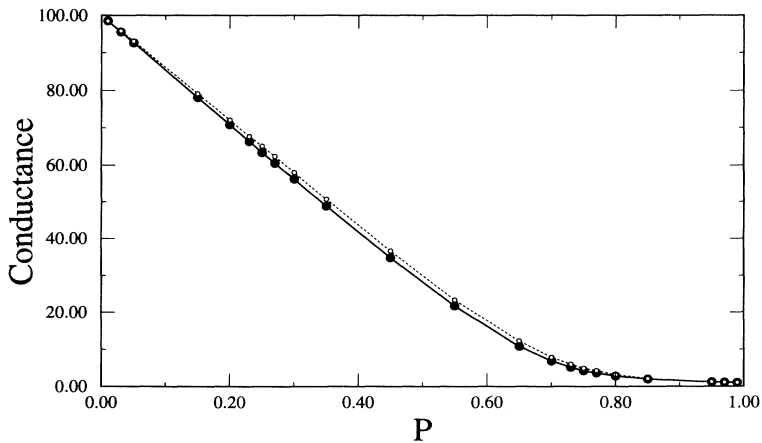

FIG. 11. The effective conductance of cubic lattices prior to any bond breaking. The data are for $g=100$. The open symbols are for $L=10$ (50 configurations), while the solid symbols are for $L=20$ (20 configurations).
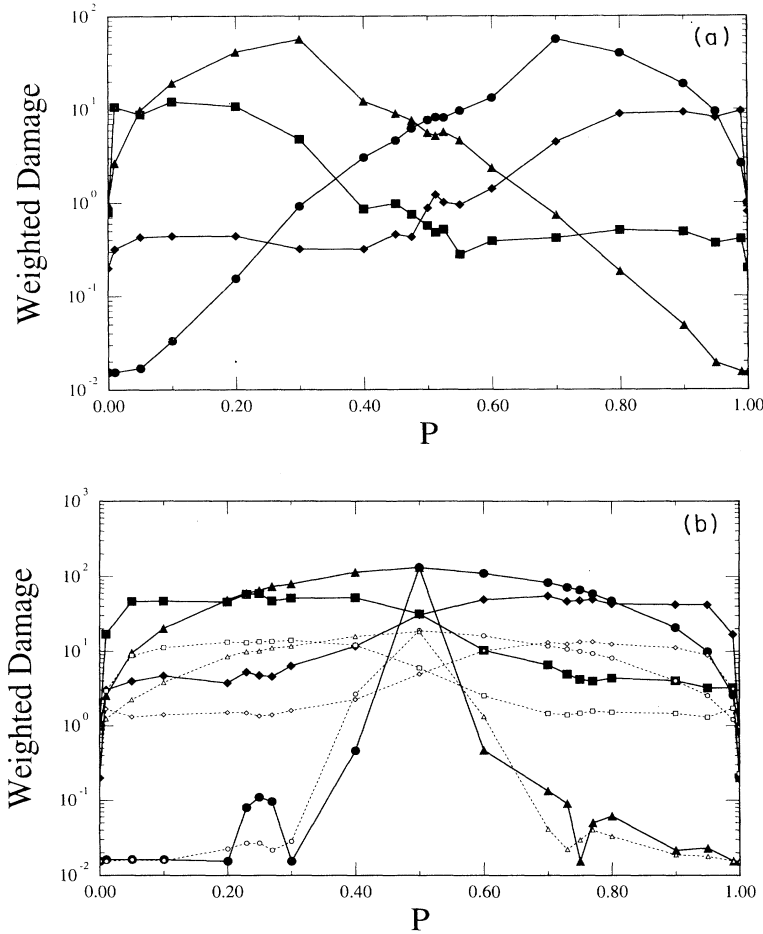
FIG. 12. The weighted damage n_w as a function of p. (a) Square lattices with $L=100$ (20 configurations) and (b) cubic lattices with $L=10$ (open symbols, 50 configurations) and $L=20$ (solid symbols, 20 configurations). In both figures $g=4, i=\frac{1}{4}$ (circles); $g=4, i=4$ (squares); $g=\frac{1}{4}, i=\frac{1}{4}$ (diamonds); $g=\frac{1}{4}, i=4$ (triangles).

portant variable, and the presence of preexisting voids plays a critical role in the composite response. Consideration of these factors and the effect of anisotropic inclusions, such as fibers and platelets, on composite behavior are the focus of our current studies.

ACKNOWLEDGMENTS

APPENDIX A

It is a standard student problem in electrostatics to show that the electric field near the tip of a wedge or funnel of dielectric constant ϵ_1 placed in a background of dielectric constant ϵ_2 is singular on approach to the wedge tip as[25] (in 2D)

$$E_\perp \sim a(l)\frac{E_0}{r^\nu} \ , \tag{A1}$$

where $E_\perp$ is the electric field perpendicular to the axis of

the wedge, E_0 is the applied electric field, r is the radial distance from the crack tip, and ν is an exponent which depends on the two dielectric constants and the wedge angle. $a(l)$ is a function which depends on the linear size of the defect. Similarly, when a low-conductivity wedge is placed in a higher-conductivity matrix there is a similar singularity in the electric field and current density at the wedge apex. In that case it is easy to show (by solving Laplace's equation in a manner similar to the electrostatic case) that the exponent ν_w is related to the conductance ratio and wedge angle ϕ via the transcendental equation

$$\sigma_0 \tan(\nu_w \phi/2) = -\sigma_1 \tan[\nu_w(\pi-\phi/2)] \ . \tag{A2}$$

In general, this must be solved numerically to find ν_w, but in the important case $\phi=\pi/2$, Eq. (A2) may be solved to find (using $g=\sigma_1/\sigma_0$) Eq. (7) of the text. Similarly, a funnel-shaped low-conductivity region placed in a higher-conductivity background has an electric-field singularity at its apex, with the exponent ν_f given by the solution to[22] (in 2D)

$$\sigma_0 \tan(\nu_f \phi/2) = \sigma_1 \cot[\nu_f(\pi/2-\phi/2)] \ . \tag{A3}$$

Again, this may be explicitly solved in the case $\phi=\pi/2$, with the result (8) of the text. In three dimensions, solids

of revolution formed from wedges and funnels again show electric-field singularities at their apexes, with the exponents given by solutions to transcendental equations involving Legendre polynomials.[22]

If the defect is finite and on a lattice, the electric field at the apex scales as

$$E_{apex}/E_0 \sim i_{apex}/i_0 \sim 1 + cl^\nu , \qquad (A4)$$

where c is a constant of order 1. Numerical simulations of lattice defects support this conclusion.[23] Similar results apply to the case of high-conductivity wedges or funnels placed in low-conductivity backgrounds. The most singular electric fields occur when, in the case of low-conductivity wedges or funnels, the apex points perpendicular to the direction of the applied field, while for high-conductivity funnels or wedges, the apex points in the direction of the applied field.

As in the case of random voids,[6] we argue that the largest field-enhancing wedge or funnel sets the typical scale of the largest local current enhancement in the network. The area (2D case) of a wedge is given by

$$A = l^2 \tan(\phi/2) . \qquad (A5)$$

Now we consider the case of a high-conductivity matrix, with a small volume fraction $(1-p)$ of low-conductivity bonds randomly placed in it. The probability of finding a wedge of size A is then approximately

$$P_A \sim L^2 (1-p)^A . \qquad (A6)$$

The typical largest wedge in a network of size A is then found by setting $P_A = 1$, which yields

$$A_{max} \sim \frac{-2\ln L}{\ln(1-p)} . \qquad (A7)$$

The typical largest current in the network is given by combining (A2) and (A5) with (A6) so that

$$i_{max} \sim i_0 \left[1 + c \left[\frac{-2\ln L}{\tan(\phi/2)\ln(1-p)} \right]^{\nu/2} \right] . \qquad (A8)$$

Assuming that failure at this current scale leads to overall failure, this then implies

$$I_b(p) \sim \frac{I_b(0)}{1 + c[-2\ln L /\tan(\phi/2)\ln(1-p)]^{\nu/2}} \qquad (A9)$$

as quoted in Eq. (6) of the text.

The above results can easily be extended to different conductance ratios, to the case of dissimilar dielectric constants, and to elastic wedges and funnels, and hence to random elastic networks.[26] In all cases the predicted size effect in the dilute limit is logarithmic with an exponent in the logarithm which depends on the modulus ratio.

APPENDIX B

As found in the simulations, the major damage mechanism is the failure of the weaker of the two phases of the composite. This mechanism is most effective when the weak phase is highly conducting (stiffer in the analogous elastic problem), as the strong phase is strongly connected across the sample, so that cracks do not propagate from the weak phase. However, there is a damage mechanism which occurs when strong, particulate, highly conducting inclusions are placed in a weaker, less conducting matrix (in the elastic case this is analogous to strong stiff inclusions embedded in a softer weaker matrix). In that case, failure first occurs in the matrix at the ends of needlelike, strong highly conducting inclusion. This is because there is a strong electric-field concentration near the ends of highly conducting needles and funnels, as described in Appendix A. However, when the funnels, wedges, and needles are highly conducting, the strongest electric-field concentration occurs when the apex is oriented along the direction of the applied field. However, a crack wants to propagate *perpendicular* to the direction of the applied field. Thus damage first occurs at the apex of funnels, but the initial damage can be stable. We have checked that this mechanism operates for a range of needles and funnels. There is an applied current I_i at which the region near the defect apex fails but is stable, and a second (for $g > 4$) current I_b at which a crack is unstable and propagates from the site of the initial damage.

We now develop a scaling argument for the damage which should occur in *random networks* due to the tip-sealing damage mechanism outlined in the paragraph above. Clearly, the ratio of the two current scales $R = I_b/I_i$ is important, and no tip-sealing damage should occur for $R < 1$. It is also known that for large currents the distribution of bond currents in a random resistor network with conductance ratio g (prior to any damage) is approximated by a "shrunk exponential"

$$P(i) \sim \exp\left[-c \left[\frac{i}{i_0} \right]^{2/\nu} \right] , \qquad (B1)$$

where c is a constant and ν is an exponent less than 1, which can be estimated by considering various ideal defect structures, as described in Appendix A. To make direct contact with Appendix A, we can find the typical largest current in a random resistor network by setting

$$L^d \exp\left[-c \left[\frac{i_{max}}{i_0} \right]^{2/\nu} \right] = 1 , \qquad (B2)$$

which implies

$$\frac{i_{max}}{i_0} \sim \left[\frac{d \ln L}{c} \right]^{\nu/2} , \qquad (B3)$$

which is asymptotically equivalent to Eq. (6). Here i_0 is the applied current while I_0 is the failure current in the absence of the funnel. As before, I_i is the applied current at which the apex bond fails, so that $i_{max}/i_0 = I_0/I_i$

Based on Eq. (B1), it is straightforward to estimate the amount of damage caused by tip sealing. Assuming the damage is random and the distribution of currents (B1) is unaffected by the damage, we have

$$n_{mat} \sim L^2 \int_{i_b/i_0}^{\infty} \exp[-c(i/i_0)^{2/\nu}]di , \qquad (B4)$$

where $i_b/i_0 = I_0/I_b$ is the current enhancement in the

bond which fails just prior to catastrophic failure. For large I_0/I_b, Eq. (B4) is approximately

$$n_{mat} \sim L^2 \exp\left[-c\left[\frac{I_i}{I_b}\frac{I_0}{I_i}\right]^{2/\nu}\right].$$ (B5)

Using Eq. (B3), we then find

$$n_{mat} \sim L^x$$ (B6)

with

$$x \sim d\left[1 - \left[\frac{I_i}{I_b}\right]^{2/\nu}\right],$$ (B7)

as quoted in Eq. (5) of the text. The main point to be taken from Eq. (B7) is that the matrix damage has an exponent which varies continuously with g through the ratio I_i/I_b. The smaller the ratio I_i/I_b, the larger the damage prior to instability.

[1]Y. S. Li and P. M. Duxbury, Phys. Rev. B **40**, 4889 (1989).

[2]P. M. Duxbury and S. G. Kim, in *Mechanical Properties of Porous and Cellular Materials,* edited by D. Green, K. Sieradzki, and L. J. Gibson, MRS Symposia Proceedings No. 207 (Materials Research Society, Pittsburgh, 1991), p. 179.

[3]P. M. Duxbury, in *Statistical Models for the Fracture of Disordered Media* edited by H. J. Herrmann and S. Roux (North-Holland, New York, 1990).

[4]P. M. Duxbury, P. D. Beale, H. Bak, and P. A. Schroeder, J. Phys. D **23**, 1546 (1990).

[5]P. M. Duxbury, P. L. Leath, and P. D. Beale, Phys. Rev. B **36**, 367 (1987).

[6]P. L. Leath and W. Xia, Phys. Rev. B **44**, 9619 (1991).

[7]P. D. Beale and P. M. Duxbury, Phys. Rev. B **37**, 2785 (1988).

[8]W. A. Curtin, J. Am. Ceram. Soc. **74**, 2837 (1991); S. L. Phoenix and R. Raj, Acta Metall. Mater. **40**, 2813 (1992).

[9]S. G. Kim and P. M. Duxbury, J. Appl. Phys. **70**, 3164 (1991).

[10]*Statistical Models for the Fracture of Disordered Media* (Ref. 3).

[11]See, e.g., *Proceedings of the Third International Conference on the Fundamentals of Fracture* [Mater. Sci. Eng. A **176** (1994)].

[12]Z. Hashin, J. Appl. Mech. **50**, 481 (1983).

[13]S. Feng, B. I. Halperin, and P. N. Sen, Phys. Rev. B **35**, 197 (1987).

[14]D. Hull, *An introduction to composite materials* (Cambridge University Press, Cambridge, England, 1981).

[15]D. G. Harlow and S. L. Phoenix, J. Mech. Phys. Solids **39**, 173 (1991); D. G. Harlow and S. L. Phoenix, Int. J. Fract. **17**, 601 (1981).

[16]P. M. Duxbury and P. L. Leath, Phys Rev. B **49**, 12 676 (1994); Phys. Rev. Lett. **72**, 2805 (1994); P. L. Leath and P. M. Duxbury, Phys. Rev. B **49**, 14 905 (1994).

[17]C. Moukarzel and P. M. Duxbury, J. Appl. Phys. **76**, 4086 (1994).

[18]See D. Stauffer, *Introduction to percolation theory* (Taylor and Francis, London, 1985), p. 17.

[19]L. de Arcangelis, S. Redner, and H. J. Herrmann, J. Phys. (Paris) Lett. **46**, L585 (1985).

[20]J. S. Langer, Phys. Rev. A **3123**, (1992); A. Yuse and M. Sano, Nature **362**, 329 (1993); E. Louis and F. Guinea, Phys. Rev. B **49**, 994 (1994).

[21]R. L. Smith, Proc. R. Soc. London Ser. A **382**, 179 (1982).

[22]J. Machta and R. A. Guyer, Phys. Rev. B **36**, 2142 (1987).

[23]P. M. Duxbury, R. A. Guyer, and J. Machta, Phys. Rev. B (to be published).

[24]See, e.g., I. C. Kim and S. Torquato, Phys. Rev. B **43**, 3198 (1991), and references therein.

[25]See, e.g., J. D. Jackson, *Classical Electrodynamics,* 2nd ed. (Wiley, New York, 1975), Sec. 2.11.
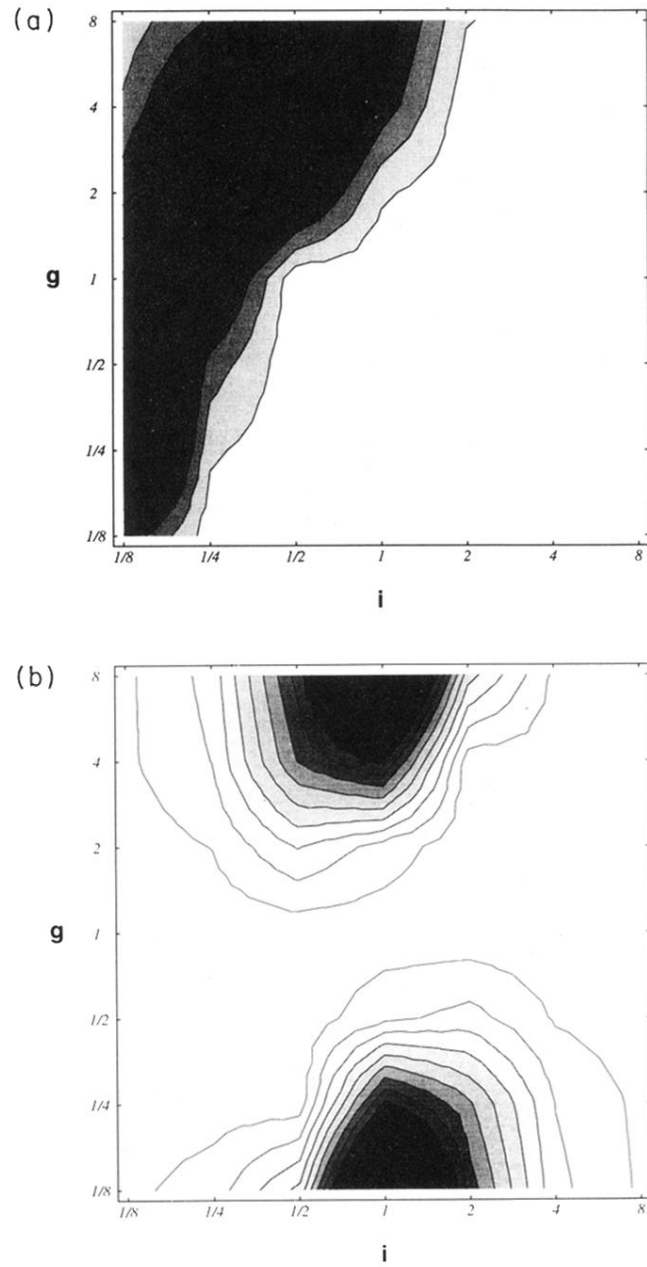
[26]S. K. Chan and J. Machta (unpublished).

FIG. 4. Weighted damage (n_w) maps (see text) for $L = 100$ square lattices at (a) $p = 0.75$ and (b) $p = 0.50$. The averages are over 10 configurations. The white level corresponds to $n_w < 8.3$ (a), and 4.5 (b), while the darkest level corresponds to $n_w > 91.2$ (a) and 49.5 (b), and the gray scale is linear.
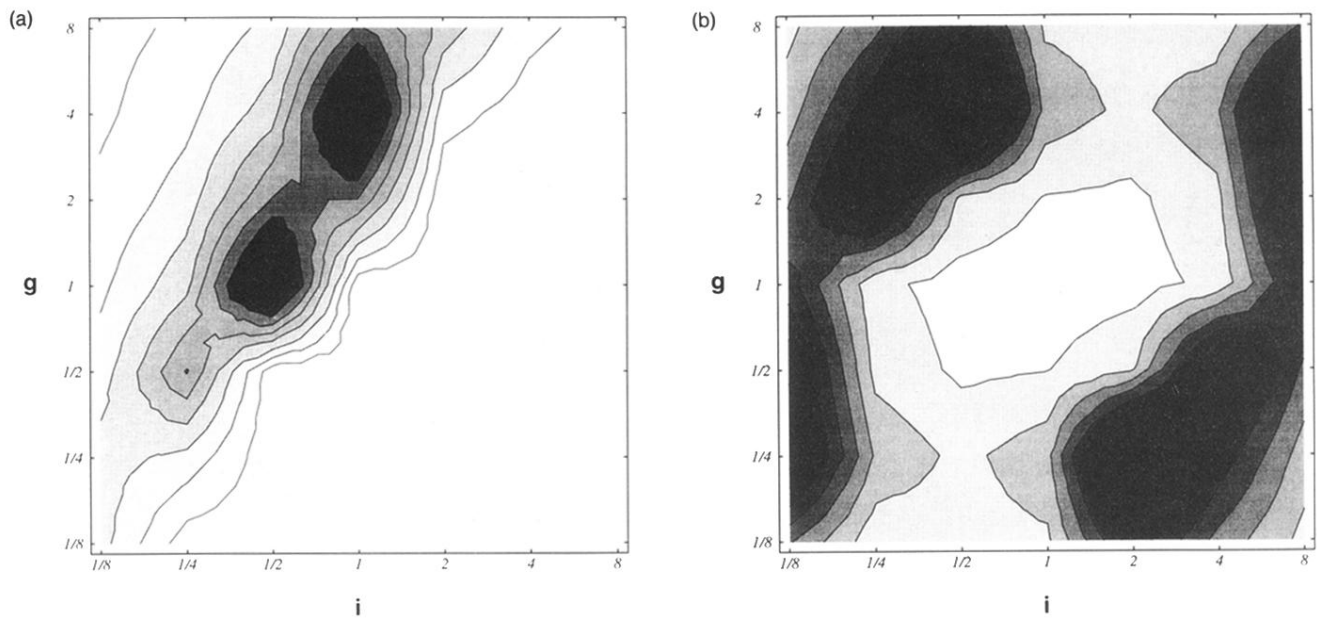
FIG. 5. Weighted damage (n_w) maps (see text) for cubic lattices at (a) $p=0.85$ ($L=15,20$ configurations) and, (b) $p=0.50$ ($L=20,10$ configurations). The white level corresponds to $n_w < 9.17$ (a) and 20.5 (b), while the darkest level corresponds to $n_w > 100.8$ (a) and 225.5 (b), and the gray scale is linear.